PHYSICAL REVIEW A **93**, 020501(R) (2016)

Precision measurement of the electron affinity of niobium

Zhihong Luo,[1] Xiaolin Chen,[1] Jiaming Li,[1] and Chuangang Ning[1,2,*]

[1]*Department of Physics, State Key Laboratory of Low-Dimensional Quantum Physics, Tsinghua University, Beijing 10084, China*

[2]*Collaborative Innovation Center of Quantum Matter, Beijing, China*

(Received 4 November 2015; published 17 February 2016)

Due to the low cross section of p-wave threshold photodetachment and the complicated electronic structures, the uncertainty of electron affinities for many transition elements still remains around 10 meV, which has not been improved for three decades. In this study, the electron affinity of Nb is measured as 917.40(6) meV or 7399.35(50) cm^{-1} using the slow electron velocity imaging method. The accuracy was improved by a factor of more than 400 with respect to the previous measurement. Furthermore, the fine structures of Nb^- were successfully resolved: 16.87(12) meV ($^5D_1$), 46.75(12) meV ($^5D_2$), 86.85(12) meV ($^5D_3$), and 156.00(37) meV ($^5D_4$) above the ground $^5D_0$, respectively.

DOI: 10.1103/PhysRevA.93.020501

Electron affinity (EA) is one of the fundamental properties of an atom, which is defined as the energy released when an electron is added to a neutral atom. Thanks to the development of new experimental methods and the availability of narrow-linewidth lasers, the atomic EA measurement has been steadily improved [1–3]. The typical uncertainty of EA values for the main group elements is 0.01-0.05 meV. These values are mainly obtained by the laser photodetachment threshold (LPT) method established in 1970 [4]. With the LPT method, Neumark *et al.* reported the very precise binding energy of O^- with a relative uncertainty of 5×10^{-7} [5]. This was considered as a reference standard for more than a decade. Using the LPT method, Haugen and co-workers have reported many precise EA values [6–11]. Recently, with the pioneering work by Blondel and co-workers using the laser photodetachment microscopy (LPM) method [12], the uncertainties for O^-, OH^-, Se^-, and Ge^- go down even to the 1 μeV level [13–16]. However, for many transition metal anions with a partially filled d subshell, no significant improvement has been reported during the past 30 years after the pioneering work by Lineberger and co-workers in 1981 [17]. The measurement accuracy for the electron affinities of many transition metal atoms remains around 10 meV before this study. For example, EA values of V, Nb, and Ta are 0.526(12), 0.894(25), and 0.323(12) meV, respectively [17]. The experimental EA data for most of the lanthanides and actinides are not available yet [2]. There are three difficulties in conducting these experiments: (1) the photodetachment cross section for the p-wave detachment is very low, according to the Wigner threshold law $\sigma \propto (E_k)^{3/2}$ [18]. Here, σ is the photodetachment cross section, and E_k is the photoelectron kinetic energy. (2) The complicated electronic structures of the transition metal anions require a very high energy resolution to resolve the fine structures. In this study, the energy resolution needs to be better than 1 meV to resolve all transitions of Nb^-. Otherwise, it is difficult to make unambiguous assignment for the transitions, such as the study of Ce^- [19]. (3) Some transitional metals oxidize readily in the conventional laser ablation ion source. It is difficult to get a high-intensity anion beam, especially for those elements with relatively lower EA values. The early experiment successfully generated Nb^- ions using the cesium sputtering ion source [17]. However, its continuum working mode is not suitable for the pulsed lasers with a low repetition rate.

In the present work, the slow electron velocity imaging (SEVI) technique developed by Newmark *et al.* was employed to conduct the precision measurement of the EA value of Nb [20,21]. SEVI has an impressive high resolution for low-energy electrons [20–23]. Recently, an energy resolution 1.2 cm^{-1} for $E_k = 5.2\,cm^{-1}$ has been reported by Wang and co-workers [22]. Note that 1 eV = 8065.544 005(50) cm^{-1}, as recommended by 2014 CODATA [24]. The ground-state configuration of Nb^- is $(4d^4 5s^2)\ ^5D_0$, while the ground-state configuration of Nb is $(4d^4 5s)\ ^6D_{1/2}$. The electric dipole transition results in a p-wave detachment around the threshold. As mentioned earlier, the p-wave photodetachment cross section near the threshold is very low. It would be extremely difficult to apply the LPM method for the EA measurement of Nb, since the highly accurate LPM method relies on the measurement right above the photodetachment threshold. The typical photoelectron energy E_k is lower than 1 cm^{-1}. Hence, there is no LPM report for p-wave photodetachment. It is true that increasing the photoelectron kinetic energy could improve the signal-noise ratio. For example, the signal intensity for $E_k = 45\ cm^{-1}$ is 302 ($45^{3/2}$) times stronger than that for $E_k = 1\ cm^{-1}$. However, the interference rings, the essential information of the LPM method, cannot be obtained at such a high kinetic energy. For the LPT method, E_k may go up to $\sim$100 cm^{-1}. The LPT method has been applied to several transition metal elements [8–10]. However, the LPT method cannot resolve the congested p-wave photodetachment channels with a separation less than 20 cm^{-1} due to the zero-slope onset at the threshold. Moreover, a significant systematic deviation from the Wigner threshold law may deteriorate the accuracy of the LPT method, which has been observed in the Ir^- and Pt^- studies [10]. Fortunately, the SEVI method could overcome limitations resulting from threshold laws.

Figure 1 shows the schematic diagram of the experimental apparatus. The apparatus includes three major sections: a laser ablation ion source, a Wiley-McLaren type time-of-flight (TOF) mass spectrometer, and a photoelectron velocity-map imaging system. The second harmonic output (532 nm) of

*ningcg@tsinghua.edu.cn

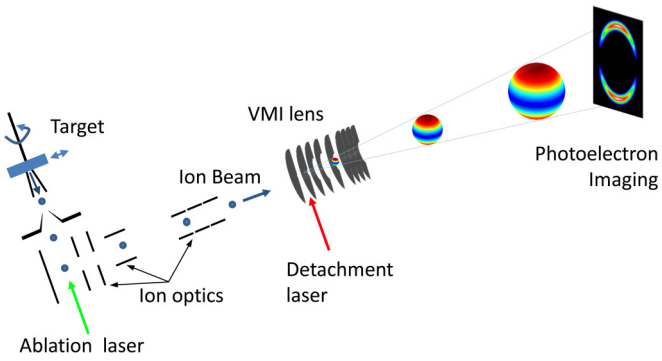

FIG. 1. Schematic view of the photoelectron spectroscopy apparatus for mass-selected anions using the velocity-map imaging (VMI) method. A mass gate and a rotatable ion detector in the front of the VMI lens are not shown.

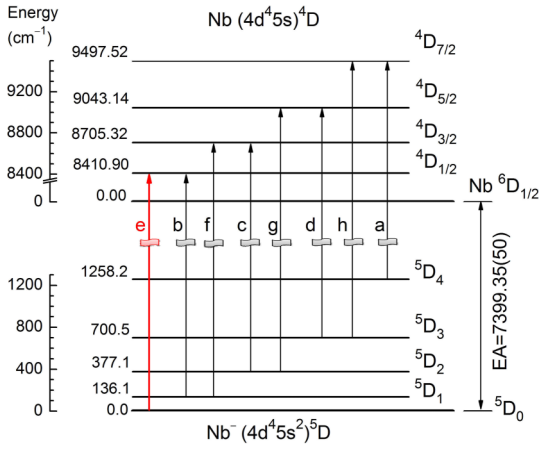

FIG. 2. Energy levels of Nb and Nb$^-$ related to the present measurement. The ground state of Nb is $^6D_{1/2}$. The ground state of Nb$^-$ is $^5D_0$. The labels of each transition are the indexes of the observed peaks in Fig. 3. The transition e, Nb($^4D_{1/2}$) ← Nb$^-$($^5D_0$), is used for the electron affinity measurement.

a Nd:YAG laser is focused onto a continually rotating and translating Nb metal disk to produce the anions. The NbO^-, NbO_2^-, and NbO_3^- signals are often the dominant species in the ion beam because Nb oxidizes readily. An in-line sodium oven is used to introduce the sodium vapor to get rid of the trace oxygen and water contamination in the source cell and the carrier helium gas. A small piece of metallic sodium is placed in the gas line. The gas line is heated by a cartridge heater. The Nb oxides' signals gradually vanished after turning on the sodium oven, while the intensity of Nb^- was enhanced for several times. The Nb^- ions are then accelerated by a −900 V high-voltage pulse in the TOF mass spectrometer. The mass resolution $(M/\Delta M)$ of the current design is 300 for $M\sim100$. The target ion species are selected by the mass gate and detected by an in-line microchannel plate detector. The ion detector is rotatable. It can be moved out of the ion path during the subsequent photoelectron imaging measurement. The velocity-map imaging (VMI) lens system is similar to the design from Ref. [22], which was originally used by the ion imaging experiment [25,26]. The selected ion species enter the VMI lens system through a 6-mm-diameter aperture on the repeller plate and are perpendicularly crossed by the detachment laser beam in the interaction zone. The detached photoelectrons are projected onto a phosphor screen behind a set of microchannel plates and recorded by a CCD camera. A real-time intensity-weighted centroid program is used to determine the hitting position of each photoelectron. The raw imaging data are reconstructed through an inverse Abel transformation [27]. A tunable detachment laser system is also essential for performing the high-resolution SEVI experiments. Our SEVI apparatus is equipped with a Spectra-Physics dye laser system (400-920 nm, linewidth 0.06 cm^{-1} at 625 nm) pumped by a Quanta-Ray Pro 290 Nd:YAG laser (20 Hz, 1000 mJ/pulse at 1064 nm). The photon energy ($h\nu$) is further measured by a HighFinesse WS6-600 wavelength meter with an accuracy of 0.02 cm^{-1}.

The imaging system is optimized using the iodine anion I^- as the test sample, because a high photoelectron count rate is readily achieved due to the s-wave photodetachment around its threshold. The energy resolution obtained is 0.56 cm^{-1} for $E_k = 1.38$ cm^{-1}, and 5.1 cm^{-1} for $E_k = 93.6$ cm^{-1} at an imaging voltage of −40 V. In order to record the full spectra in the Nb^- study, a higher imaging voltage of −150 V is used. The energy resolution is 3.8 cm^{-1} for $E_k = 45.6$ cm^{-1}, which is the typical E_k for the present EA measurement.

Figure 2 shows the energy levels of Nb^- and Nb involved in the present measurement. The previous study reported that the photodetachment energy from the anion ground state Nb$^-$($^5D_0$) to the neutral ground state Nb($^6D_{1/2}$) is 0.894 eV (wavelength $\lambda = 1369$ nm) [17], which is out of the tuning range of the dye laser system. The neutral Nb atomic energy levels are well known with a high accuracy. This gives freedom to choose the photodetachment final neutral state. This flexibility is crucial for the current Nb study and other elements with a low EA value, such as Ca with a very low EA value of 24.55(10) meV [28]. After a careful search, the Nb($^4D_{1/2}$) ← Nb$^-$($^5D_0$) channel with the photodetachment threshold wavelength $\lambda \approx 630$ nm is ideal for conducting the Nb EA measurement. The energy levels for the ^4D term of Nb are 8410.90, 8705.32, 9043.14, and 9497.52 cm^{-1} for $J = 1/2, 3/2, 5/2$, and $7/2$, respectively, relative to the neutral ground state Nb($^6D_{1/2}$) [29]. The label of each transition in Fig. 2 corresponds to the observed peaks in Fig. 3. The spectrum assignment was made based on the calculation results of the anion and the experimental neutral levels. The transition intensities could be estimated by combining the 9-J symbol calculations, the Wigner threshold law, and thermal population [7,30].

Figure 3 shows the photoelectron images and spectra obtained at photon energy $h\nu = 15750.95$, 15855.83, and 16 494.63 cm^{-1}, respectively. Each photoelectron image is obtained with 300000 laser shots. The photoelectron angular distributions clearly show a parallel transition, which are consistent with the expected p-wave detachment. The binding energy spectra show transitions $a - d$ in Fig. 3(a); transitions $b - e$ in Fig. 3(b); transitions $b - h$, in Fig. 3(c). The interval between peaks c and d is only 15.6 cm^{-1}. They are clearly resolved in Fig. 3(b), in which $h\nu = 15\,855.83$ cm^{-1}, but are significantly overlapped in Fig. 3(c), in which $h\nu = 16\,494.63$ cm^{-1}. This comparison clearly shows the

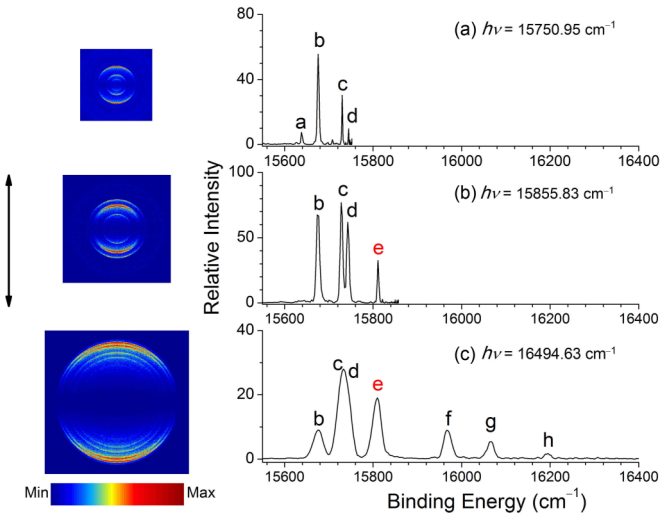

FIG. 3. Photoelectron images and spectra of Nb^- at photodetachment energies of (a) 15 750.95 cm^{-1}, (b) 15 855.83 cm^{-1}, and (c) 16 494.63 cm^{-1}. The double arrow indicates the laser polarization. Peak *e* is a result of photodetachment Nb($^4D_{1/2}$) ← Nb^-($^5D_0$), which is used to determine the electron affinity of Nb. See Fig. 2.

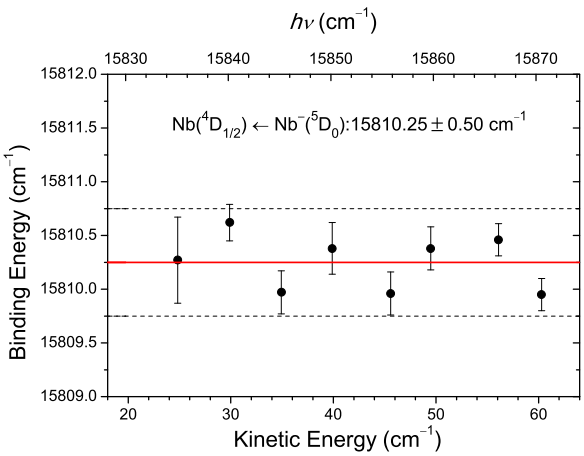

FIG. 4. Binding energy of Nb($^4D_{1/2}$) ← Nb^-($^5D_0$) transition as a function of the kinetic energy of photoelectrons. The dotted lines indicate the ±0.5 cm^{-1} uncertainty.

importance of conducting the low-E_k photodetachment experiment. The only channel originated from the anion ground state Nb^-($^5D_0$) is transition *e* [Nb($^4D_{1/2}$) ← Nb^-($^5D_0$)], so it was selected as the target channel for the present EA measurement. The peak assignments and measured transition energies are listed in Table I. The fine structure of the Nb^-(^5D) can be derived from the measurements. The splitting of Nb^-($^5D_1$ ← $^5D_0$) is determined as 136.1(10) cm^{-1} according to the interval between peaks *b* and *e*. The splitting of Nb^-($^5D_2$ ← $^5D_0$) is 377.1(10) cm^{-1} according to the interval between peaks *c* and *e*, and the energy difference between $^4D_{3/2}$ and $^4D_{1/2}$ of Nb. Similarly, we obtained 700.5(10) cm^{-1} for Nb^-($^5D_3$ ← $^5D_0$). Peak *a*(Nb $^4D_{7/2}$ ← Nb^- $^5D_4$) is extremely weak, which is probably due to a low population and a short lifetime of $^5D_4$ state compared with the time of flight 0.3 ms from the ion source cell to the photodetachment zone. In order to determine the energy level of $^5D_4$, 600 000 laser shots were accumulated at $h\nu$ = 15 750.95 cm^{-1}. To confirm the assignment, the fine structures of Nb^- were calculated using the spin-orbit coupling multireference configuration interaction method with the TZP-DKH basis set. The TZP-DKH basis set was obtained from the basis set exchange website [31]. The calculations were carried out using the MOLPRO package. As shown in Table I, the calculated splittings are significantly lower than the experimental results. However, the scaled calculations agree well with the experimental results.

TABLE I. Measured binding energies and fine structures of Nb^-, and the electron affinity of Nb.

Peak	Levels (Nb ← Nb^-)	Binding energy (cm^{-1})
a	$^4D_{7/2}$ ← $^5D_4$	15638.7(30)
b	$^4D_{1/2}$ ← $^5D_1$	15674.3(8)
c	$^4D_{3/2}$ ← $^5D_2$	15727.6(8)
d	$^4D_{5/2}$ ← $^5D_3$	15742.0(8)
e	**$^4D_{1/2}$ ← $^5D_0$**	**15810.25(50)**
f	$^4D_{3/2}$ ← $^5D_1$	15968.4(12)
g	$^4D_{5/2}$ ← $^5D_2$	16065.9(11)
h	$^4D_{7/2}$ ← $^5D_3$	16194.6(20)

Fine structures of Nb^- (cm^{-1})

Levels	Calculated[a]	Experimental
$^5D_1$ ← $^5D_0$	96 (123)	136.1(10)
$^5D_2$ ← $^5D_0$	292 (374)	377.1(10)
$^5D_3$ ← $^5D_0$	575 (736)	700.5(10)
$^5D_4$ ← $^5D_0$	969 (1240)	1258.2(30)

EA(Nb) = 7399.35(50) cm^{-1} or 917.40(6) meV

[a]The value in the parentheses is the scaled one with a factor of 1.28.

The energy difference between the different neutral Nb states can also be extracted from the eight transitions. It is worth comparing them with the standard atomic data. As an example, the interval between peaks *b* and *f* is 294.1(14) cm^{-1}, in an excellent agreement with the energy difference 294.42 cm^{-1} between $^4D_{1/2}$ and $^4D_{2/3}$ of neutral Nb. Similarly, we have an interval 338.3(14) cm^{-1} between peaks *c* and *g* vs 337.82 cm^{-1} between $^4D_{3/2}$ and $^4D_{5/2}$, and 452.6(20) cm^{-1} between peaks *d* and *h* vs 454.38 cm^{-1} between $^4D_{5/2}$ and $^4D_{7/2}$. These accurate data can be considered as the fingerprints of atomic states for the unambiguous assignment.

A primary measurement of the transition energy of channel *e* can help us to narrow down the range for performing a series of low-E_k photoelectron measurements to achieve a high accuracy of EA value. The photon energy was scanned from 15835 to 15 870 cm^{-1} with a step around 5 cm^{-1}. Hence, the photoelectron energy E_k for channel *e* varied from 25 to 60 cm^{-1}. Figure 4 shows the binding energy of transition *e* plotted as a function of E_k. The centers of these observed peaks were obtained using a Gaussian function fitting procedure. Table I lists the assignments and the energies of these peaks. The mean binding energy of peak *e* is 15810.25 cm^{-1} with an uncertainty ±0.50 cm^{-1}. The uncertainty is mainly contributed from the fitting procedure to obtain the peak center due to the low count rate. By subtracting the energy 8410.90 cm^{-1} of Nb($^4D_{1/2}$), the electron affinity of Nb is obtained as

7399.35(50) cm^{-1} or 917.40(6) meV, which is consistent with the previously reported value of 894(25) meV [17], but the accuracy is improved by a factor of more than 400. On the theoretical side, the early calculation suggested EA(Nb) = 0.82 eV [32]. A more recent calculation reported a value of 0.99 eV [33]. Both studies have significant deviations. The accurate experimental EA(Nb) value determined in this study could serve as a benchmark for developing more accurate theoretical methods for transition metals.

In summary, the application of the SEVI method to the photodetachment study of Nb^- has significantly improved the accuracy of the electron affinity of Nb. The fine-structure components of the Nb^- $(4d^45s^2)$ ^5D ground state were also successfully resolved and measured. The present experimental technique not only removes the limitation of the measurement around the p-wave photodetachment threshold, but also provides a sufficient energy resolution for resolving the congested photodetachment channels. It makes it possible to improve the EA measurement accuracy to sub-cm^{-1} for nearly all transition metal atoms.

ACKNOWLEDGMENTS

This work is supported by National Natural Science Foundation of China (NSFC) (Grant No. 91336104) and Ministry of Science and Technology of China (MOST) (Grant No. 2013CB922004) of the National Key Basic Research Program of China.

Z.L. and X.C. contributed equally to this work.

[1] W. C. Lineberger, Annu. Rev. Phys. Chem. **64**, 21 (2013).
[2] T. Andersen, Phys. Rep. **394**, 157 (2004).
[3] T. Andersen, H. K. Haugen, and H. Hotop, J. Phys. Chem. Ref. Data. **28**, 1511 (1999).
[4] W. C. Lineberger and B. W. Woodward, Phys. Rev. Lett. **25**, 424 (1970).
[5] D. M. Neumark, K.R. Lykke, T. Andersen, and W. C. Lineberger, Phys. Rev. A **32**, 1890 (1985).
[6] M. Scheer, R. C. Bilodeau, and H. K. Haugen, Phys. Rev. Lett. **80**, 2562 (1998).
[7] M. Scheer, R.C. Bilodeau, C. A. Brodie, and H. K. Haugen, Phys. Rev. A **58**, 2844 (1998).
[8] R. C. Bilodeau, M. Scheer, and H. K. Haugen, J. Phys. B **31**, 3885 (1998).
[9] M. Scheer, C. A. Brodie, R. C. Bilodeau, and H. K. Haugen, Phys. Rev. A **58**, 2051 (1998).
[10] R. C. Bilodeau, M. Scheer, H. K. Haugen, and R. L. Brooks, Phys. Rev. A **61**, 012505 (1999).
[11] R. C. Bilodeau and H. K. Haugen, Phys. Rev. Lett. **85**, 534 (2000).
[12] C. Blondel, C. Delsart, and F. Dulieu, Phys. Rev. Lett. **77**, 3755 (1996).
[13] C. Blondel, C. Delsart, C. Valli, S. Yiou, M. R. Godefroid, and S. Van Eck, Phys. Rev. A **64**, 052504 (2001).
[14] C. Delsart, F. Goldfarb, and C. Blondel, Phys. Rev. Lett. **89**, 183002 (2002).
[15] M. Vandevraye, C. Drag, and C. Blondel, Phys. Rev. A **85**, 015401 (2012).
[16] D. Bresteau, P. Babilotte, C. Drag, and C. Blondel, J. Phys. B: At., Mol. Opt. Phys. **48**, 125001 (2015).
[17] C. S. Feigerle, R. R. Corderman, S. V. Bobashev, and W. C. Lineberger, J. Chem. Phys. **74**, 1580 (1981).
[18] E. P. Wigner, Phys. Rev. **73**, 1002 (1948).
[19] J. Felton, M. Ray, and C. C. Jarrold, Phys. Rev. A **89**, 033407 (2014).
[20] A. Osterwalder, M. J. Nee, J. Zhou, and D. M. Neumark, J. Chem. Phys. **121**, 6317 (2004).
[21] D. M. Neumark, J. Phys. Chem. A **112**, 13287 (2008).
[22] I. León, Z. Yang, H. T. Liu, and L. S. Wang, Rev. Sci. Instrum. **85**, 083106 (2014).
[23] H. T. Liu, C. G. Ning, D. L. Huang, P. D. Dau, and L. S. Wang, Angew. Chem., Int. Ed. **52**, 8976 (2013).
[24] P. J. Mohr, D. B. Newell, and B. N. Taylor, arXiv:1507.07956.
[25] A. T. J. B. Eppink and D. H. Parker, Rev. Sci. Instrum. **68**, 3477 (1997).
[26] W. Li, S. D. Chambreau, S. A. Lahankar, and A. G. Suits, Rev. Sci. Instrum. **76**, 063106 (2005).
[27] B. Dick, Phys. Chem. Chem. Phys. **16**, 570 (2014).
[28] V. V. Petrunin, H. H. Andersen, P. Balling, and T. Andersen, Phys. Rev. Lett. **76**, 744 (1996).
[29] J. E. Sansonetti and W. C. Martin, J. Phys. Chem. Ref. Data **34**, 1559 (2005), or NIST Atomic Spectra Database version 5.0, 2012, http://www.nist.gov/pml/data/asd.cfm.
[30] P. C. Engelking and W. C. Lineberger, Phys. Rev. A **19**, 149 (1979).
[31] https://bse.pnl.gov.
[32] L A. Cole and J. P. Perdew, Phys. Rev. A **25**, 1265 (1982).
[33] P. Calaminici and R. Mejia-Olvera, J. Phys. Chem. C **115**, 11891 (2011).